Journal of Chromatography A, 1218 (2011) 6531–6539

Contents lists available at ScienceDirect

Journal of Chromatography A

journal homepage: www.elsevier.com/locate/chroma

Numerical modeling of the elution peak profiles of retained solutes in supercritical fluid chromatography

Krzysztof Kaczmarski[a,*], Donald P. Poe[b], Georges Guiochon[c,d]

[a] Department of Chemical and Process Engineering, Rzeszów University of Technology, Ul. W. Pola 2, 35-959 Rzeszów, Poland
[b] Department of Chemistry and Biochemistry, University of Minnesota Duluth, Duluth, MN 55812, USA
[c] Department of Chemistry, University of Tennessee, Knoxville, TN 37996-1600, USA
[d] Division of Chemical Sciences, Oak Ridge National Laboratory, Oak Ridge, TN, USA

ARTICLE INFO

Article history:
Received 15 April 2011
Received in revised form 29 June 2011
Accepted 7 July 2011
Available online 20 July 2011

Keywords:
Supercritical fluid chromatography
Column efficiency
Peak profiles
Porosity distribution
Expansion cooling
Heat balance
Heat transfer

ABSTRACT

In supercritical fluid chromatography (SFC), the significant expansion of the mobile phase along the column causes the formation of axial and radial gradients of temperature. Due to these gradients, the mobile phase density, its viscosity, its velocity, its diffusion coefficients, etc. are not constant throughout the column. This results in a nonuniform flow velocity distribution, itself causing a loss of column efficiency in certain cases, even at low flow rates, as they do in HPLC. At high flow rates, an important deformation of the elution profiles of the sample components may occur. The model previously used to account satisfactorily for the retention of an unsorbed solute in SFC is applied to the modeling of the elution peak profiles of retained compounds. The numerical solution of the combined heat and mass balance equations provides the temperature and the pressure profiles inside the column and values of the retention time and the band profiles of retained compounds that are in excellent agreement with independent experimental data for large value of mobile phase reduced density. At low reduced densities, the band profiles can strongly depend on the column axial distribution of porosity.

1. Introduction

Supercritical fluid chromatography (SFC) is considered as a "green" alternative to classical liquid chromatography due to its use of a mobile phase based on high-density CO_2. Even though organic solvents must often be added to CO_2 as modifiers, their required concentrations are lower than in HPLC. Other advantages of SFC are the possibility of an easy adjustment of the solvent properties by changing the operating pressure and the temperature. The efficiency of a column in SFC, compared to that of a similar system used in classical HPLC, is generally higher, due to lower mass transfer resistances. For these reasons SFC often permits the achievement of faster and more efficient separations than HPLC.

The desire to decrease the separation times of mixtures leads to increases in the mobile phase flow rate. This means that the columns must be run with a high pressure gradient. A large pressure drop along a column is not desirable because the temperature of the mobile phase decreases when it expands. Then, the mobile phase tends to absorb heat from the air outside the column. As a result, axial and radial temperature gradients form inside the column. These temperature gradients cause corresponding axial and radial gradients of all the physico-chemical parameters. The phenomena observed in the SFC column are similar to those encountered in ultra high pressure liquid chromatography (UHPLC). For large back pressures (e.g., 500 bar and more in UHPLC and several dozen bars in SFC) the deformations of the peak shapes are similar – compare the experimental peak profiles in [1,2]. The difference is that in UHPLC the heat is generated inside the column due to viscous friction whereas in SFC the heat is absorbed from the column surroundings. As a result, the gradients of physico-chemical parameters are in the opposite direction in both versions of chromatography [3,4]. The other important difference is that the axial and the radial mobile phase density gradients are much greater in the case of SFC. Because the density has a crucial impact on the adsorption isotherm in SFC, the density gradients can have a significant impact on retention and efficiency.

Most SFC separations are performed using outlet pressures around 150 bar. The peak deformations noted above, however, are generally important only when columns are operated at temperatures and pressures slightly above the critical conditions, at outlet pressures below about 130 bar, temperatures up to about 100 °C, and reduced densities close to 1.0. These conditions tend to be accompanied by excess efficiency losses and are typically avoided in general practice [5]. This is unfortunate because the mass transport properties of carbon dioxide under these conditions

* Corresponding author. Tel.: +4817 865 12 95; fax: +4817 854 36 55.
E-mail addresses: kkaczmarski@prz.edu.pl, kkaczmarski@prz.rzeszow.pl (K. Kaczmarski).

0021-9673/$ – see front matter © 2011 Elsevier B.V. All rights reserved.
doi:10.1016/j.chroma.2011.07.022

favor faster, more efficient separations. Attempts to model chromatographic behavior under these conditions have thus far been unsuccessful [6,7]. A model that is valid over the entire range of potentially useful conditions in SFC could be beneficial by providing a basis for exploiting these conditions. The work presented in this paper addresses this serious deficiency by presenting an accurate model that satisfactorily describes chromatographic behavior under these severe conditions.

Due to the similarity of the physical phenomena taking place in SFC, the method developed for modeling the UHPLC peak profiles can be used also for modeling those in SFC. We previously developed and validated a model combining the heat and the mass balance equations of UHPLC columns, an isotherm model for the solute, and the equation accounting for flow in porous media [8,9]. This model accurately predicts analyte retention factors, their elution band profiles, and the dependence of the column efficiency on the mobile phase velocity. On the basis of this model described in the first part of our earlier paper [4], a general SFC model coupling the heat and the mass balance equations with an appropriate equation of state was proposed. The numerical solution of the generalized ED model coupled with the calculated temperature and pressure distributions enabled excellent forecasts of the retention times and efficiency for the elution of an unsorbed solute [4].

The goal of this work was to adapt and validate this model for retained solutes. We restricted our investigation to analytical scale of SFC. A new version of this model which enables analyses of the impact of the axial porosities distributions on the temperature, the flow rate and the concentration band profiles is proposed. To validate this model, we first compared the temperature recorded along the column wall and the pressure drop along the column with those calculated with our model. The agreement is excellent. Afterwards we compare the simulated peaks profiles for several retained and unretained solutes, for average carbon dioxide reduced density (RD) equal to 1.5 and 1.0. In the first case a good agreement between the experimental results and the calculated ones was obtained. In the second case the agreement is good at very low and very high flow rates. However, at medium mobile phase flow rates, some discrepancies between theory and experiments are observed.

2. Mathematical models

The mathematical model of SFC applied in this paper is very similar to that used in the first part of our earlier work [4]. The SFC model combines three separate models: (1) a model of heat transfer; (2) a model of mass transfer; and (3) a model of mobile phase velocity distribution. The heat transfer model is exactly the same as in previous paper [4] and will not being discussed here. The second model accounts for the propagation of a solute band along a column in which there are gradients of temperature, viscosity, velocity, density. It also includes other parameters, ignored previously, which can change along the column or in the radial direction, namely the packing heterogeneity. We apply our mass balance model on columns in which there is a gradient of packing density or in other words a gradient of external porosity. The existence of axial packing density gradients was mentioned by Wong et al. [10]. These authors found that the external porosity decreases along the column. The existence of a radial packing heterogeneity follows from experiments that point out a radial distribution of the flow rate obtained at low mobile phase velocity [11], that is for flow rates for which viscous friction heat effects could be neglected.

The mass transfer model was coupled with an isotherm model, the equilibrium constants of which depend on the local temperature and the mobile phase density.

The assumption of a bed heterogeneity forces modifications of the third model previously used, which accounts for the distribution of the mobile phase velocity. In this work, we assumed that the flow rate depends on the local temperature, the pressure, the viscosity and the density of the mobile phase as well as on the bed porosity.

2.1. The mass balance equation

In writing the mass balance for an analyte, we assumed that the contributions to band broadening due to the finite mass transfer resistances and to the axial dispersion can be lumped into an apparent dispersion coefficient. We assumed that this coefficient can be evaluated using formulae developed in [9,12] and used in [4], in spite of the fact that the porosity is a function of the position inside the column. It should be also remembered that axial dispersion, radial dispersion and the velocity are functions of the position inside the column. Under this assumption, the mass balance equation is an extension of the equilibrium-dispersive (ED) model [4,13].

The mass balance equation of the generalized ED model is written as follows:

$$\frac{\partial C_A}{\partial t} + F\frac{\partial q_A}{\partial_t} + \frac{1}{\varepsilon_t}\frac{\partial(uC_A)}{\partial z} = -\frac{\partial}{\partial z}(J_Z) - \frac{1}{r}\frac{\partial}{\partial r}(rJ_r) \tag{1}$$

where the axial and the radial components of the mass flux are

$$J_z = -D_{z,a}\frac{\partial C_A}{\partial_z} \tag{2}$$

$$J_r = -D_{r,a}\frac{\partial C_A}{\partial r} \tag{3}$$

The C_A and q_A are the analyte concentrations in the mobile and stationary phases at equilibrium (g/L), respectively, t is the time, z is the axial coordinate, u is the axial superficial mobile phase velocity, $D_{z,a}$ and $D_{r,a}$ are the local axial and radial apparent dispersion coefficients (m^2/s), respectively, $F = (1-\varepsilon_t)/\varepsilon_t$ is the phase ratio and ε_t is the total porosity of the column, which can be a function of the axial and the radial positions. In the model, the convective mass transfer in the radial direction was neglected – the numerical experiments proved that it has no influence on the concentration band profiles.

The dispersion terms in Eqs. (2) and (3) follow from Fick's first law, namely the diffusion flux in Fick's law as depicted by the expression:

$$J = -D_m \nabla C_A \tag{4}$$

It would be more theoretically justified to express the diffusion flux by the mass fraction [14]:

$$J = -D_m \rho \nabla\left(\frac{C_A}{\rho}\right) \tag{5}$$

where D_m is the molecular diffusion coefficient and ρ is the fluid density. However, the differences between the peak profiles calculated with the first and the second equations were marginal in our case, so in the following, we refer the dispersion terms to the concentration C_A.

The apparent axial dispersion coefficient was calculated from the following equation [4]:

$$D_{z,a} = \frac{D_L\varepsilon_e}{\varepsilon_t} + \left(\frac{k_1}{1+k_1}\right)^2 \frac{u^2 d_p}{\varepsilon_t \varepsilon_e F_e 6}\left[\frac{d_p}{10D_{\text{eff}}} + \frac{1}{k_{\text{ext}}}\right] \tag{6}$$

where

$$k_1 = F_e\left(\varepsilon_p + (1-\varepsilon_p)\frac{\delta q_A}{\delta C_A}\right); \quad F_e = \frac{1-\varepsilon_e}{\varepsilon_e}; \quad D_{\text{eff}} = \frac{D_m\varepsilon_p}{\tau} \tag{7}$$

and D_L is the axial dispersion coefficient, d_p is adsorbent diameter, D_{eff} is effective particle diffusivity, ε_e is the external porosity, which can depend on the position inside column, ε_p is the particle

porosity, τ is the tortuosity coefficient and k_{ext} is the external mass transfer coefficient.

As in part one of our work [4], the apparent radial dispersion coefficient, $D_{a,r}$, was calculated on the basis of the plate height equation derived by Knox [15,16]:

$$D_{r,a} = \frac{0.03 d_p u}{\varepsilon_t} + 0.7 D_m \tag{8}$$

We assumed that this equation can be used for a heterogeneous bed. In Eq. (8), D_m is the molecular diffusion coefficient and d_p is the adsorbent particle diameter.

The axial dispersion coefficient, D_L, was approximated by the relationship [13]:

$$D_L = \gamma_1 D_m + \gamma_2 u d_p \tag{9}$$

where γ_1 and γ_2 are geometrical constants. The first term in Eq. (9) accounts for molecular diffusion and the second for eddy diffusion. It was assumed that $\gamma_1 = 0.7$ [13] whereas γ_2 was estimated from the experimental data.

The remaining parameters in Eqs. (6) and (7), k_{ext}, D_m, and τ, were calculated as described later in Section 2.4. It should be noted that all the dispersion and diffusion coefficients are functions of the position inside the column.

The model (1) was solved with the typical initial and boundary conditions listed in our earlier work [4]. Only the boundary conditions for the column center, $r = 0$, and the internal column wall radius $r = R_i$ were changed to the following ones:

For $t > 0$, $r = R_i$ and $r = 0$

$$J_r = 0 \tag{10}$$

Eq. (7) must be combined with an appropriate isotherm equation. In this work, we applied the model proposed by Martire and Boehm [17] (Eqs. (103) and (104) in their paper). According to these authors, the dependence of the retention factor k on the reduced density and the reduced temperature reads

$$\ln(k) = c_0 + \frac{c_1}{T_R} + c_2 \rho_R + c_3 \frac{\rho_R}{T_R} + c_4 \frac{\rho_R^2}{T_R} \tag{11}$$

where ρ_R is the reduced density and T_R is the reduced temperature. The parameters c_0–c_4 are adjustable parameters and must be estimated from experimental data. Taking into account the definition of the retention factor the following expression is obtained:

$$q_A = C_A \frac{\varepsilon_t}{1 - s_t} \exp\left(c_0 + \frac{c_1}{T_R} + c_2 \rho_R + c_3 \frac{\rho_R}{T_R} + c_4 \frac{\rho_R^2}{T_R} \right) \tag{12}$$

It should be noted that from Eq. (12) it follows that the local concentration in the stationary phase is a function of the local values of the mobile phase density and the temperature.

2.2. Mobile phase velocity distribution and pressure calculation

In a previous paper we assumed a homogenous column bed. In this work, we recognize the heterogeneous porosity distribution in the radial and/or the axial direction. Taking this into account we have to modify the equation for the local value of the mobile velocity developed in [8].

Following the method presented in [8] it is easy to find that the local value of the mobile phase velocity should be calculated from Eq. (13):

$$U_z(r,z) = \frac{u^o \rho^o}{\eta(r,z)(\overline{\rho/\eta})_z} \frac{\varepsilon_e(r,z)^3}{(1 - \varepsilon_e(r,z))^2} \tag{13}$$

where η is the viscosity, $(\overline{\rho/\eta})$ denotes the average value at a given axial position, of the expression ρ/η multiplied by $\varepsilon_e^3/(1-\varepsilon_e)^2$,

$$\left(\frac{\bar{\rho}}{\eta}\right)_z = \frac{2}{R_i^2} \int_0^R \frac{\rho(r,z)}{\eta(r,z)} \frac{\varepsilon_e(r,z)^3}{(1 - \varepsilon_e(r,z))^2} r \, dr \tag{15}$$

and u^o, ρ^o are the mobile phase superficial velocity and density at the column inlet.

The local pressure gradient was calculated according to the correlation developed by Blake, Kozeny, and Carman [14], using the following equation:

$$-\frac{\delta P}{\delta z} = \xi \frac{u^o \rho^o}{d_p^2 (\overline{\rho/\eta})_z} \tag{16}$$

where ξ is an empirical parameter generally considered as equal to 150 [14].

The above system of equations has to be closed by the following relationship:

$$\Delta P = \int_0^L \left(-\frac{\delta P}{\delta z} \right) dp \tag{17}$$

where ΔP is the actual pressure drop along the column, measured from the instrument gauges and L is the column length.

The radial mobile phase velocity, u_r, was computed numerically from the continuity equation [8]:

$$\frac{1}{r} \frac{\partial}{\partial r} (\rho r u_r) + \frac{\partial (\rho u_z)}{\partial r} = 0 \tag{18}$$

The radial mobile phase velocity was so small that it had no influence on the band profiles, so it is neglected in the following.

2.3. Methods of calculation of the physico-chemical parameters

The methods of calculation of the physico-chemical parameters were identical to those used in our previous paper [4].

2.3.1. Heat transfer

The carbon dioxide density and its heat capacity were calculated by the method described by Span and Wagner [18], the viscosity and the thermal conductivity were calculated according to models presented by Fenghour et al. [19] and Vesovic et al. [20] respectively. The effective conductivity was calculated from a correlation developed by Zarichnyak and Novikov [21] for a two-component heterogeneous system that has a chaotic structure.

2.3.2. Mass transfer

To solve the mass balance equation discussed above, the local values of the external mass transfer coefficient, k_{ext}, and the molecular diffusivity, D_m, must be calculated. As in our previous paper, the coefficient k_{ext} was obtained from the Wilson and Geankoplis correlation [22], and the molecular diffusion coefficient D_m was estimated from the Wilke–Chang equation with modified constants [23].

Finally, the tortuosity parameter, τ, needed to evaluate the effective particle diffusion parameter was calculated from the correlation [13]:

$$\tau = \frac{(2 - \varepsilon_p)^2}{\varepsilon_p} \tag{19}$$

2.4. Method of calculation of numerical solutions of the models

The coupled system of the mass balance and the heat balance equations was solved using a method previously described in detail in [8]. First, the steady-state distributions of the temperature and the pressure throughout the column were derived. Afterwards, the

time dependent mass balance equation was solved, using the temperature and the pressure profiles previously obtained. The heat balance and the differential mass balance equations were solved using the method of orthogonal collocation on finite elements (OCFE) in its analog version previously described [24]. The spatial derivatives were discretized following the OCFE method. The set of ordinary differential equations obtained through this process was then solved using the VODE solver [25].

3. Experimental work

3.1. Apparatus

The SFC instrument consisted of an ISCO 260D syringe pump, a helium-actuated Valco injector with a 0.50-μL internal sample loop, a Hewlett–Packard 5790 gas chromatograph with a flame ionization detector and a high-pressure nitrogen back pressure system. The injector was placed inside the column oven and samples dissolved in liquid carbon dioxide were introduced from a pressurized reservoir. The instrument has previously been described in greater detail [1].

Data were acquired using a high-speed chromatography data acquisition system (VG Data Systems Chromatography Server, 22-bit A/D conversion rate at 960 Hz) and the Thermo LabSystems XChrom software. The sampling frequency was varied from 30 to 240 Hz depending on the flow rate to provide at least 30 data points over the half-width of the narrowest peak. All peaks were analyzed using the manual integration utility included with the software.

A 2.0 mm × 150 mm column with stainless steel walls and fittings, packed with Spherisorb C8 (Waters Corporation, Milford, MA 01757, USA) was used. This is the same physical column used previously with this solute system in this series of studies [1,4]. The average particle diameter was 5 μm. The external column diameter was 6.4 mm. A total porosity of 0.724 was measured by pycnometry. We assumed an external porosity of 0.400 for the column, yielding ξ equal about 150 in the Blake, Kozeny, and Carman equation.

The column was exposed to the oven air with the fan operating in the typical fashion. The column connections were made with 0.18-mm i.d. stainless steel tubing, with a length of 100 mm between the injector and column inlet, and 50 mm between the column outlet and the flow splitter for the detector. The overall extracolumn volume was found experimentally to be 4.3 μL. The extracolumn variance for the solute mixture was measured at 50 °C and RD = 1.2 over the flow rates of interest. The resulting data were used to estimate the contribution of the extracolumn hardware to the total peak variance in the test chromatograms at 50 °C. For all retained solutes at RD = 1.0 the extracolumn variance was less than 1% of the total peak variance at all flow rates used. At RD = 1.5 and flow rates of 0.100, 0.500 and 1.500 mL/min, the corresponding average percentages were 0.4%, 1.9% and 5.5%.

3.2. Column surface temperature

The temperatures at various points on the column were measured to the nearest 0.01 K using a series of self-adhesive RTD (resistive thermal device) probes. The RTDs were calibrated against a Fisher Digital Thermometer traceable to NIST standards with a certified accuracy of ±0.05 K. For the 150-mm column, probes were placed directly on the column wall at z = 25, 50, 75, 100 and 125 mm, where z is the distance from the column inlet. Two other probes at z = 0 and z = 150 mm measured the endfittings temperature.

3.3. Chemicals

Carbon dioxide was SFC grade with no helium. Methane was 99 mol% pure. Both were obtained from Scott Specialty Gases, Troy, MI, USA. A mixture containing methane (C1), *n*-dodecane (C12), *n*-tetradecane (C14), *n*-hexadecane (C16) and *n*-octadecane (C18) was prepared in liquid carbon dioxide. 600 μL of a neat mixture containing equal masses of the four liquid alkanes were introduced into a 150-mL stainless steel vessel. The excess air was removed by brief connection to a vacuum pump, followed by addition of methane to 1 bar. The container was then filled with carbon dioxide to 120 bar at room temperature.

3.4. Measurement of the retention factors

All separations were made as mentioned above on 5-micron Waters Spherisorb-C8 particles. The elution times were corrected for the holdup time caused by the column connectors and the fused silica restrictor connected to the FID. A constant flow rate of 0.100 mL/min set at the pump (−2.0 °C) was used in all cases. The column outlet pressure was set in conjunction with the inlet pressure to yield an average pressure corresponding to the desired mobile phase density. The column with seven RTD probes attached was suspended in the oven with the fan operating. The retention factors were measured for 26 combinations of four temperature settings (35, 40, 45, 50 °C) and seven reduced density settings (0.6, 0.8, 1.0, 1.2, 1.4, 1.6, 1.8). A reduced density of 1.8 at 45 °C and 50 °C was not accessible, due to the high pressures required. For 25 of these conditions, the measurements were performed in triplicate. For the lowest target density of RD = 0.6 the density varied between runs, resulting in three individual measurements at slightly different densities, increasing the total number of temperature–density settings to 28. It should be noted that we have to measure the retention factors for values of the reduced density as low as 0.6, because the mobile phase density can drop down inside column to such low values – see Ref. [4].

4. Results and discussion

4.1. Dependence of retention factor on density and temperature

In this work, we analyzed the retention of *n*-alkanes at the analytical scale. These solutes have been studied previously and exhibit a predictable behavior in SFC [1,17]. The dependence of the retention factor k on the reduced density and the reduced temperature was fit to Eq. (11) in the mathematical section, according to Martire and Boehm [17]. The isotherm constants, c_0–c_4 were determined over the entire range of temperatures from 308 to 323 K and reduced densities from 0.6 to 1.8, This means that for each individual component all the experimental data available were simultaneously used in the estimation of these parameters. Even at the low flow rate used for these measurements, with pressure drops of approximately 2 bar, we observed temperature drops along the column as great at 0.24 K compared to the temperature of the incoming mobile phase, mostly at reduced densities from 0.8 to 1.2. As can be seen from Eq. (11) the retention factors strongly depend on the column temperature and the mobile phase density. In the estimation of the isotherm parameters we assumed the local temperature in the column is equal to the inlet temperature. However, small deviations of the real average column temperature (even as low as 0.2 K) from the inlet temperature may have a considerable influence on the estimated results, therefore on the calculated retention times. To avoid this problem all the data points for which the temperature was more than 0.07 K below the inlet temperature were excluded from the fit, leaving 18 distinct temperature–density pairs with which the five coefficients for each solute were derived. Removing these questionable data points also improved the results as shown by the standard error of the fit for $\ln k$. The resulting coefficients are listed in Table 1a.

Table 1a
Coefficients for Eq. (11) for retention factors of the analytes, used for simulations at RD = 1.5. Fit based on data over the entire range of reduced densities from $0.6 \leq RD \leq 1.8$ for which the temperature drop was less than 0.07 K.

Solute	Standard error of fit	Coefficients for Eqs. (11) and (12)				
		c_0	c_1	c_2	c_3	c_4
C12	0.0195	−9.16 (+0.0182)[a]	16.5	1.39	−8.76	1.44
C14	0.0297	−9.42 (+0.0236)	18.1	1.46	−9.98	1.75
C16	0.0402	−8.79 (+0.0277)	18.7	0.963	−10.6	2.06
C18	0.0511	−8.17 (+0.0328)	19.2	0.428	−11.1	2.36

[a] The meaning of the offset (in parentheses) is discussed in the main text.

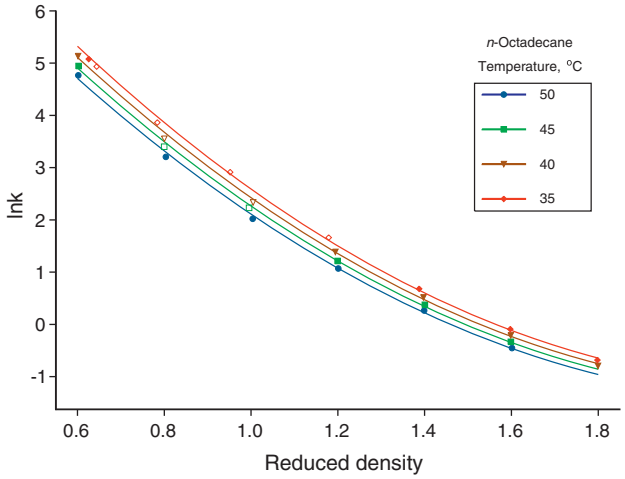

Fig. 1. Plots of the retention factors vs. the reduced density for *n*-octadecane. Solid symbols represent data used to generate the fitting coefficients in Table 1a. Open symbols show data for which the temperature drop at position $z = 100$ mm was greater than 0.07 K.

These coefficients were used for simulations at RD = 1.5. The offset for coefficient c_0 follows from observed decrease in the column retention factors over time (the experiments for RD = 1.5 were done a few months after measurements of the retention factors and the experiment for RD = 1.0).

Representative plots of the retention factors vs. the reduced density, calculated according to the values of the coefficients presented in Table 1a appear in Figs. 1 and 2. Data points that were excluded from the fit are shown in a different format (see caption).

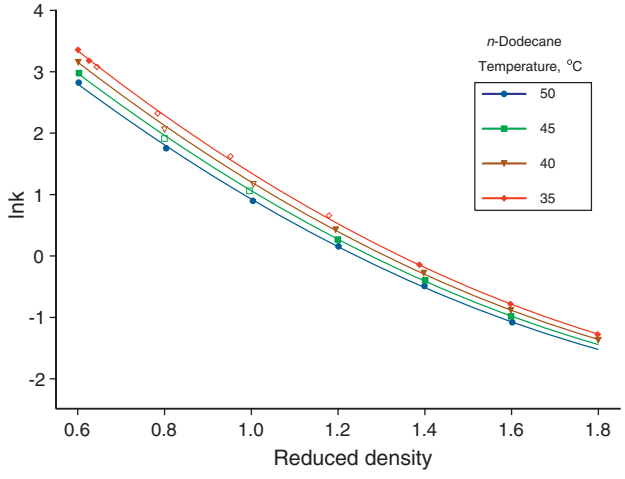

Fig. 2. Plots of the retention factors vs. the reduced density for *n*-dodecane. See Fig. 1 for explanation of symbols.

Because of the relatively large temperature drops near reduced density 1.0, a second fit was done for this region. Numerical simulations showed that the column wall temperature at $z = 100$ mm was a good indicator of the average mobile phase temperature in the column. Based on the corrected temperature data, new fits were generated using all the experimental data, including those that had been initially rejected on the basis of significant deviations between the average column temperature and the inlet temperature. The results were somewhat improved, but the experimental k values near RD = 1.0 were still significantly lower than the predicted values. We believe that these discrepancies are probably due to a competing retention mechanism. There is experimental evidence for excess adsorption of the mobile phase on the surface of the stationary phase near the critical density [26]. This may result in a perturbation of the general retention mechanism that is not addressed in the treatment by Martire and Boehm. In order to obtain a satisfactory fit for the data in the region near RD = 1.0, the data outside the range $0.6 \leq RD \leq 1.4$ were excluded. The resulting coefficients are shown in Table 1b. These fitting coefficients were then used in the simulations made for the chromatograms at RD = 1.0.

4.2. Calculation of the temperature and pressure distribution

To calculate the temperature and the pressure distributions, the heat transfer model described in our previous work [4], coupled with Eqs. (13)–(17), was solved. In a first attempt it was assumed that the column was packed uniformly with the adsorbent and that the porosities were equal to the experimental values $\varepsilon_t = 0.724$, $\varepsilon_e = 0.4$ all along the column.

To estimate the temperature distribution, three parameters are needed: the ξ parameter in the Blake, Kozeny, and Carman equation, the effective heat transfer coefficient, h_e, and the effective thermal conductivity. The last parameter was calculated with the method described in the first part of our earlier work [4]. The first and the second parameters were estimated as those that give the best agreement between the measured and the calculated outlet pressures and the column wall temperature distributions. The estimation was performed for one set of experimental data obtained for the flow rate, $F_v = 1.478$ mL/min at RD = 1.0. The estimated values were $\xi = 150.5$, $h_e = 87\ W/m^2/K$. They were used unchanged at all other flow rates and at reduced densities equal to RD = 1.5 or RD = 1.0. The representative agreement between the experimental and the theoretical values of the pressure and the temperature are shown in Table 2. For the smallest flow rate $F_v = 0.100$ mL/min, the calculated and measured outlet pressure in bars were $P_{calc} = 105.8$, $P_{exp} = 105.8$ for RD = 1.0 and $P_{calc} = 149.1$, $P_{exp} = 149.1$ for RD = 1.5. The inlet pressures were 107.5 and 151.3 respectively.

The agreement between experimental and calculated values is very good not only for the values of F_v and RD for which the parameters were estimated but for all the other combinations of F_v and RD. This result confirms that the model can correctly predict the temperature and pressure distribution in the column.

Table 1b
Coefficients for Eq. (11) for retention factors of the analytes, used for simulations at RD = 1.0. Fit based on all data over the range of reduced densities from $0.6 \leq RD \leq 1.4$.

Solute	Standard error of fit	Coefficients for Eqs. (11) and (12)				
		c_0	c_1	c_2	c_3	c_4
C12	0.0311	−8.60	16.1	0.523	−8.16	1.61
C14	0.0369	−8.09	17.0	0.0361	−9.14	2.10
C16	0.0426	−6.50	16.6	−1.41	−8.95	2.50
C18	0.0495	−5.19	16.6	−2.67	−8.96	2.91

Table 2
Comparison of the experimental and calculated column wall temperatures and outlet pressures.

Distance x [m]	Flow rate mL/min (at pump), RD = 1.0				Flow rate mL/min (at pump), RD = 1.5			
	0.638		1.478		0.5		1.5	
	T_{exp} [K]	T_{calc} [K]	T_{exp} [K]	T_{calc} [K]	T_{exp} [K]	T_{calc} [K]	T_{exp} [K]	T_{calc} [K]
0.025	322.80	322.75	322.21	322.08	323.02	322.98	322.73	322.66
0.05	322.50	322.48	321.41	321.30	322.98	322.95	322.45	322.42
0.075	322.26	322.27	320.79	320.50	322.95	322.94	322.25	322.22
0.1	321.92	322.08	319.48	319.64	322.89	322.93	321.9	322.05
0.125	321.83	321.92	318.65	318.69	322.9	322.92	321.77	321.89
x [m]	P_{exp} [bar]	P_{calc} [bar]	P_{exp} [bar]	P_{calc} [bar]	P_{exp} [bar]	P_{calc} [bar]	P_{exp} [bar]	P_{calc} [bar]
0.0	112.8	112.8[a]	120.3	120.3[a]	156.0	156.0[a]	168.7	168.7[a]
0.15	100.4	100.3	91.0	91.0	145.0	145.0	134.9	135.2

[a] Assumed values.

4.3. Retention of the unsorbed and sorbed solute – uniform porosity distribution

To validate the mass balance model presented in Section 2.1, we compared the calculated and the measured peak profiles for two experiments: the first obtained for a carbon dioxide reduced density equal to RD = 1.0 and the second for a reduced density equal to RD = 1.5. These comparisons were performed for methane, which can be regarded as unretained, and for four adsorbed compounds: *n*-dodecane, *n*-tetradecane, *n*-hexadecane and *n*-octadecane. The extracolumn holdup times were subtracted from all the elution times. Extracolumn effects on solute dispersion and band shape were assumed to be insignificant based on the small values of the extracolumn variance (see Section 3). The parameter γ_2, which appears in the second term in Eq. (9) and is related to eddy diffusion, was estimated on the basis of the experimental data. The values of this parameter are given in the captions of the figures. For clarity, we note that γ_2 is the only adjustable parameter in the mass balance model for which we need to obtain an estimate of the apparent axial dispersion coefficient $D_{z,a}$ in Eq. (6).

The calculated and the measured peaks of methane at RD = 1.0 are compared in Fig. 3. The excellent agreement between the calculated and the experimental results was obtained using the same value of the parameter γ_2 for each mobile phase velocity. This result suggests that the mobile phase flow rate distribution as well as the other parameters that influence the local velocity distribution were correctly calculated.

In Figs. 4 and 5 the experimental and the calculated peak profiles of all the analyzed species at the smallest and the highest flow rate are compared at a reduced density RD = 1.5. The dotted lines denote experimental peak profiles, the solid lines profiles calculated with the isotherm parameters in Table 1a

As can be seen, the peak profiles of the analytes calculated with the data in Table 1a are shifted slightly to the left. However, the maximum error made in the calculation of the retention times was always less than about 1%. The same accuracy of peaks reproduction was obtained for medium flow rates – figure not presented. The peak profiles of the adsorbed components calculated using the same value of γ_2 for all components and RD = 1.5 show an excellent agreement with the experimental results. The differences between the values of this coefficient and its average value for the different flow rates are less than about 15%

The next Figs. 6–8 compare the calculated (with data from Table 1b) and experimental peak profiles obtained for RD = 1.0, for all the adsorbed species.

Only for the smallest flow rates do the experimental peak profiles agree with those calculated. However, to obtain a good agreement in this case, the γ_2 have to be estimated individually for each species. In the other cases the retention times of the peak fronts were well predicted. However, the calculated retention of the tail of the peaks was always too large.

The solute velocity is highest at the column center where the temperature is the lowest and the mobile phase density is largest – see Fig. 9.

Near the column wall we have the highest temperature, the lowest fluid density and the largest retention factor.

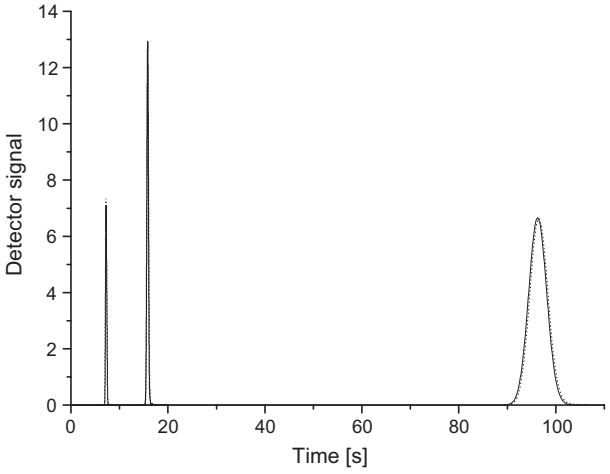

Fig. 3. Comparison of the experimental (dots) and theoretical (solid lines) band profiles at reduced density 1.0 for methane at flow rates of 1.478, 0.638 and 0.100 mL/min, from left to right. The parameter γ_2 was equal to 1.8.

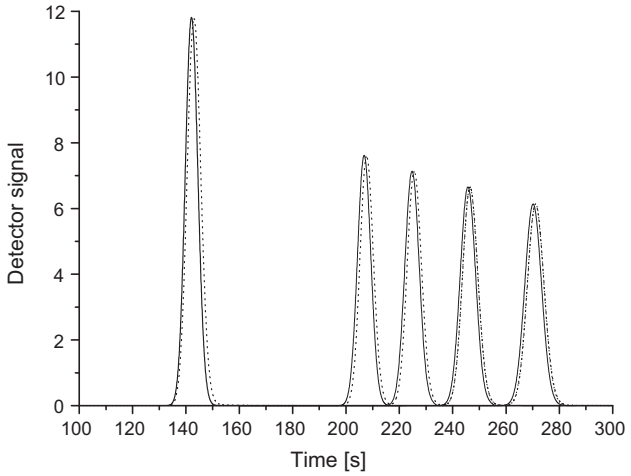

Fig. 4. Comparison of the experimental (dots) and theoretical (solid lines) peaks for C1, C12, C14, C16, C18, from left to right. Flow rate: 0.500 mL/min, RD = 1.5. The parameter γ_2 was equal to 2.5 for all the species.

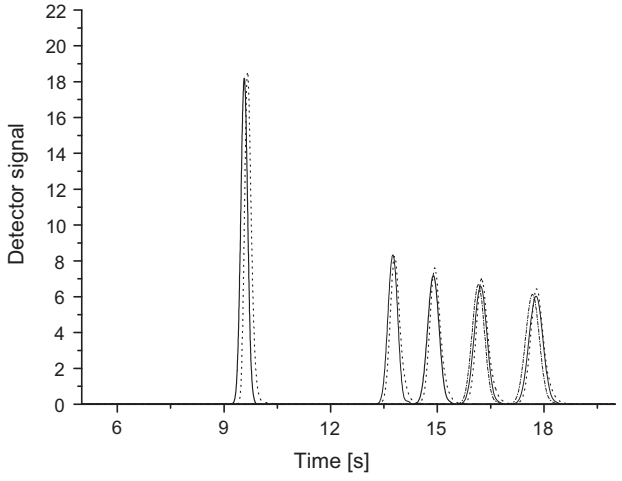

Fig. 5. Comparison of the experimental (dots) and theoretical (solid lines) peaks for C1, C12, C14, C16, C18, from left to right. Flow rate: 1.500 mL/min, RD = 1.5. The parameter γ_2 was equal to 2.7 for all the species. The meaning of the dash-dot line is explained in Section 4.4.

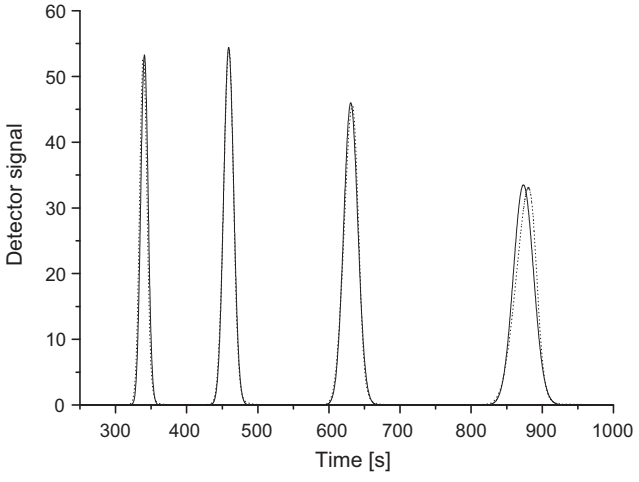

Fig. 6. Comparison of the experimental (dots) and theoretical (solid lines) peaks for C12, C14, C16, C18, from left to right. Flow rate: 0.100 mL/min, RD = 1.0. The parameter γ_2 was equal to γ_2 = 6.1, 6.5, 7, 7.7, from left to right.

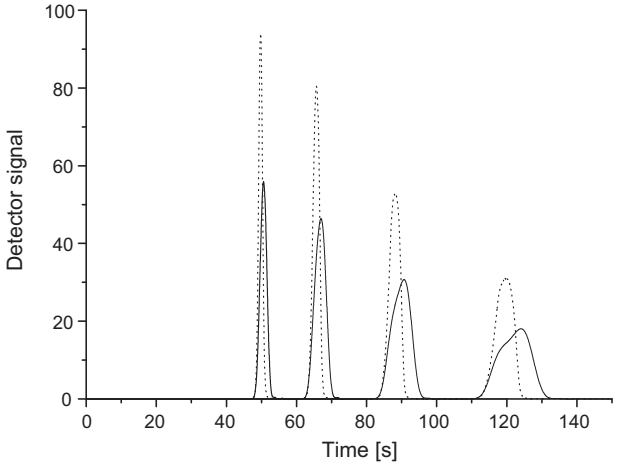

Fig. 7. Comparison of the experimental (dots) and theoretical (solid lines) peaks for C12, C14, C16, C18, from left to right. Flow rate: 0.638 mL/min, RD = 1.0. Same parameter γ_2 as in Fig. 6.

The observed discrepancy between theoretical and experimental results suggests that (i) the gradient of the calculated radial temperature is too large, (ii) the calculated flow rate of the mobile phase is too low, or (iii) the solute migrates into the column center due to a much better solubility of analytes in the denser carbon dioxide. In regard to the third possibility, in our first paper on this study [4] it was found that the difference of carbon dioxide density in the radial direction can reach several hundred kilograms/m^3 over a distance of 1 mm. (We ignore the hypothetical effect of the axial density gradient on solute migration because the axial density gradient is about 100 times smaller than the radial gradient – see Ref. [4].)

Case (i): The radial temperature gradient is determined by the measured column wall temperature and the calculated temperature in the column center. The good agreement between calculated and measured retention times of the peak fronts suggests that the temperature in the column center was correctly predicted.

Case (ii): The discrepancy between the experimental and the theoretical peak profile widths would be minimized if the flow rate near the column wall would be greater than predicted for a uniform bed. This condition would be satisfied if there would exist a gradient of external porosity, ε_e, in the radial direction – the external porosity should be greater near the wall than in the column center.

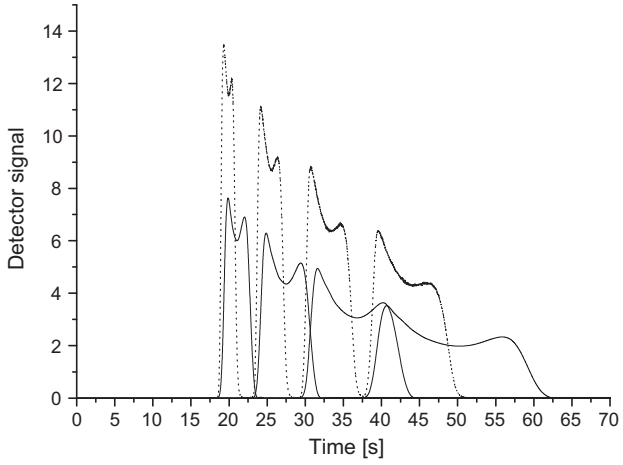

Fig. 8. Comparison of the experimental (dots) and theoretical (solid lines) peaks for C12, C14, C16, C18, from left to right. Flow rate: 1.478 mL/min, RD = 1.0. Same parameter γ_2 as in Fig. 6.

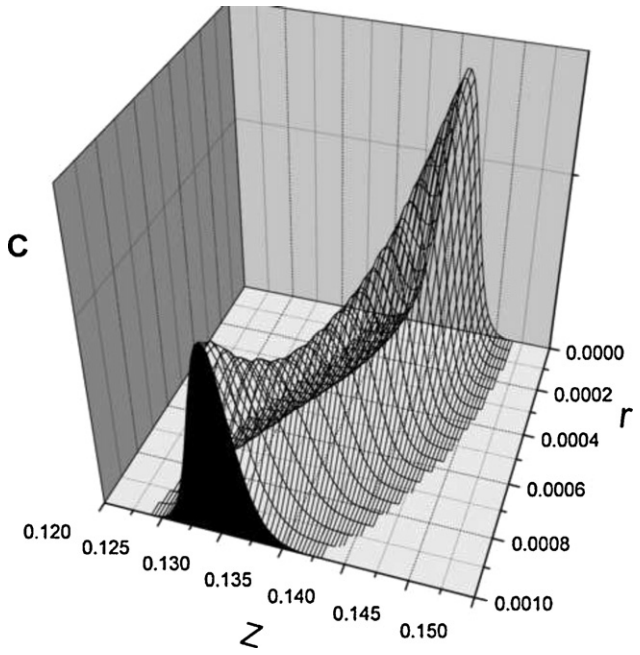

Fig. 9. Concentration band profile near column outlet calculated for solute C18. Conditions for simulation the same as in Fig. 13.

Despite the fact that, according to earlier results [11], the packing density is greater near the wall region, we did attempt to simulate peak retention assuming different radial distributions of the external porosity, with increasing porosity in the radial direction. However, the results were unsatisfactory.

Case (iii): The simulations performed for the highest flow rate show that the density of carbon dioxide can change over a distance of 1 mm, from about 360 kg/m^3 near the column wall to 480 kg/m^3 at the column center. The gradient of density should cause some solute migration toward the column center. In Supplemental Information it was explained that the mass flux in radial direction should be calculated from the expression:

$$J_r = -D_m \frac{\partial C_A}{\partial r} - C_A D_m \left(\ln(k) \frac{\partial \ln(T)}{\partial r} + \frac{\partial \ln(k)}{\partial r} \right) \quad (20)$$

The second part of the above equation is responsible for the solute migration in the radial direction. Eq. (20) was coupled with the mass transfer model, Eq. (1). However, instead of the diffusion coefficient, D_m, the radial dispersion coefficient, $D_{r,a}$, was used. However, also in this case, the results were unsatisfactory. The differences between the peak profiles calculated with and without a "radial migration term" were marginal.

4.4. Retention time of the unsorbed and sorbed solute – axial porosity distribution

The discrepancies between the experimental and theoretical band profiles that we have tried unsuccessfully to explain by the influence of a radial parameter distribution or by forces acting in the radial direction can also be explained by the axial distribution of the external porosity. Wong et al. [10] proved that the packing density increases along the column. It is smallest at the column beginning and highest at the column end. This means that we can expect a decreasing external porosity along the column. The decrease of the external porosity implies an increase of the mobile phase velocity and a decrease of the residence time of the solute near the outlet of the column. So we can expect narrower peak profiles.

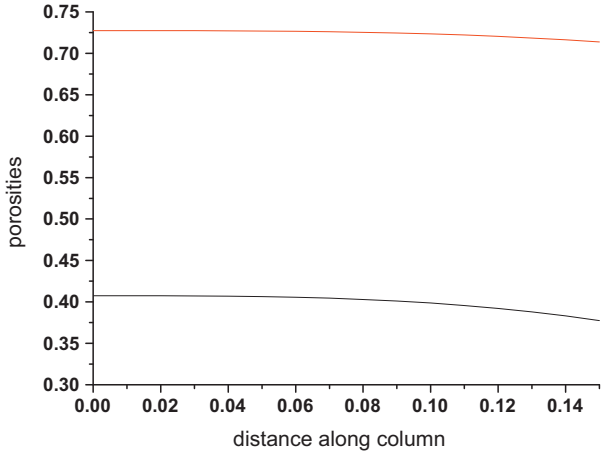

Fig. 10. The distribution of external (lower line) and total porosities (upper line) along the column.

To prove whether this hypothesis is valid, we arbitrarily assumed that the external column porosity decreases along the column according to formula:

$$\varepsilon_e = A\left(\frac{z}{L}\right)^N + B \quad (21)$$

We checked different combinations of values of the A and N parameters. The parameter B was calculated from the conditions that the average external porosity must be equal to 0.4. It means also that the total porosity have to be equal to 0.724. The best combination was: $A = -0.03$, $N = 3$, $B = 0.4075$. These values of the parameters A and N were estimated to achieve the best agreement between the theoretical and the experimental band profiles at a flow rate of $F_v = 1.478$ mL/min, for a reduced density RD = 1.0 and for the C18 component. The porosities distribution is depicted in Fig. 10. The ξ parameter in the Blake, Kozeny, and Carman equation and the effective heat transfer coefficient, h_e, were changed to the following values: $\xi = 148$ and $h_e = 60$ W/m^2/K, in order to have good agreement with the measured wall temperature and the outlet pressure.

The simulated band profiles for a reduced density equal 1.5 were almost the same as for the uniform column. The largest differences between the peaks calculated for a constant porosity and for a porosity decreasing along the column are presented in Fig. 5 – compare the solid and the dash-dot line for the components C16

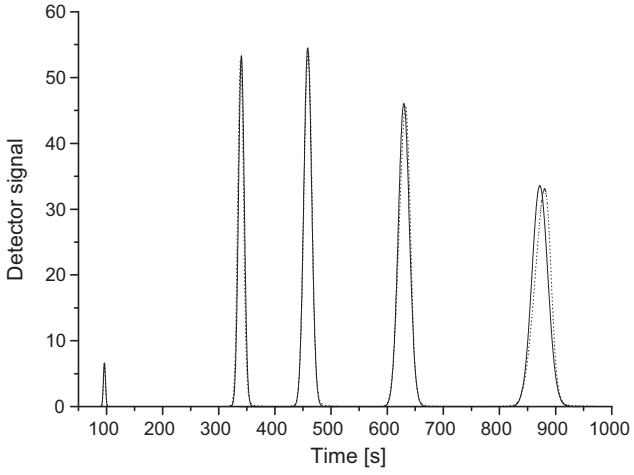

Fig. 11. Simulation of the peak profiles for RD = 1.0 at $F_v = 0.100$ mL/min, $\gamma_2 = 3.2$, 6.1, 6.5, 7, 7.7, from left to right. Components C1, C12, C14, C16 and C18, from left to right. The solid line shows the calculated, the dotted line the experimental profiles.

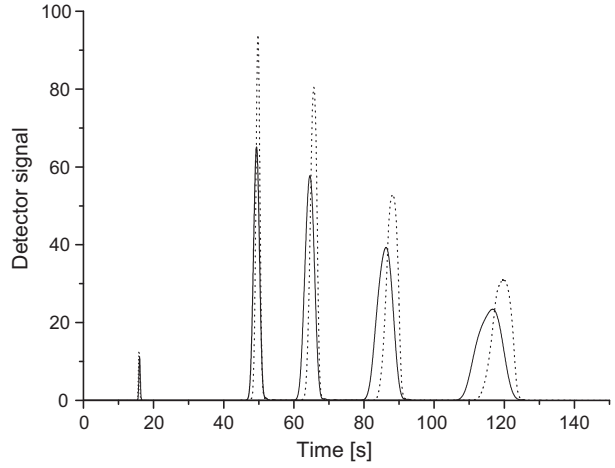

Fig. 12. Simulation of the peak profiles for RD = 1.0, at F_v = 0.638 mL/min. Same parameter γ_2 as in Fig. 11. Components C1, C12, C14, C16 and C18, from left to right. The solid line shows the calculated, the dotted line the experimental profiles.

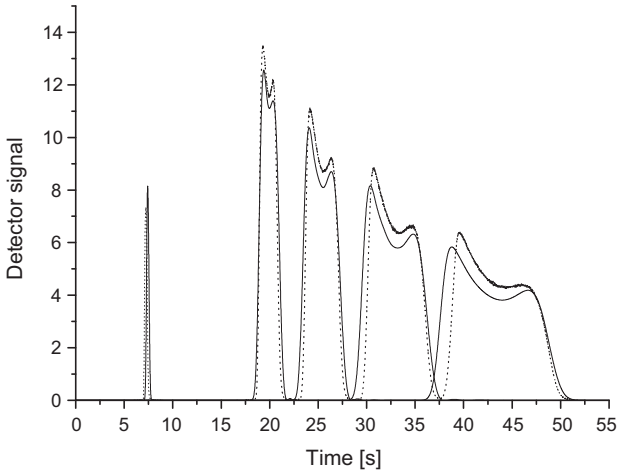

Fig. 13. Simulation of the peak profiles for RD = 1.0, at F_v = 1.478 mL/min. Same parameter γ_2 as in Fig. 11. Components C1, C12, C14, C16 and C18, from left to right. The solid line shows the calculated, the dotted line the experimental profiles.

and C18. The axial porosity distribution only marginally influences the peaks profiles at a large reduced density. However, this influence is considerable for RD = 1.0 and at the highest flow rate – compare Figs. 8 and 13. In Figs. 11–13 we compare the measured and calculated peak profiles for RD = 1.0. As can be seen, at a flow rate F_v = 0.100 mL/min the agreement is excellent, at F_v = 1.478 the agreement is still good, however, at F_v = 0.638 the experimental peaks are too wide.

The results presented illustrate how band profiles are sensitive to relatively weak changes of the external and the total porosities along the column. We did not obtain a good agreement between the experimental and theoretical profiles for all flow rates. However, from the calculations performed it follows that the axial distribution of the bed porosity has a crucial influence on the shape of the band profiles.

5. Conclusions

A general SFC model coupling the heat, the mass balance and the flow rate model is proposed. This model is a modified version of the model used in our earlier paper. This modified model can account for the axial and radial porosity distributions. Numerical solutions of the heat balance and the flow rate model predict with good agreement the column wall temperature and the pressure at the column outlet. The calculation of the temperature distribution requires the prior estimate of the external heat transfer coefficient. This coefficient can be estimated on the basis of the column wall temperature measured at the highest mobile phase flow rate.

The numerical solution of the generalized ED model coupled with the calculated temperature, the mobile phase velocity and the pressure distributions enables excellent forecasts of the retention times and the elution peaks shape of an unsorbed and sorbed solutes for a high reduced density, RD = 1.5.

It was much more difficult to model the retention of sorbed solutes at the low reduced density of RD = 1.0 and for fast flow rates. If we assume a uniform external porosity, the calculated band profiles have a shape similar to the experimental profiles but they are too wide. We analyzed several possible reasons for the discrepancies observed between the experimental and theoretical results. The most probable seems to be the impact of the axial distribution of the external porosity. Assuming that the external porosity decreases along the column, we significantly improved the modeling of the band profiles, for most but not for all the analyzed flow rates. Work to explain the elution profiles and the retention of sorbed solutes in SFC at low mobile phase reduced densities is continuing.

Acknowledgment

This work was partially supported by Grant N N204 002036 of the Polish Ministry of Science and Higher Education.

Appendix A. Supplementary data

Supplementary data associated with this article can be found, in the online version, at doi:10.1016/j.chroma.2011.07.022.

References

[1] D.P. Poe, J.J. Schroden, J. Chromatogr. A 1216 (2009) 7915.
[2] F. Gritti, G. Guiochon, J. Chromatogr. A 1216 (2009) 1353.
[3] K. Kaczmarski, F. Gritti, J. Kostka, G. Guiochon, J. Chromatogr. A 1216 (2009) 6575.
[4] K. Kaczmarski, D.P. Poe, G. Guiochon, J. Chromatogr. A 1217 (2010) 6578.
[5] T.A. Berger, Chromatographia 37 (1993) 645.
[6] H.G. Janssen, H.M.J. Snijders, A. Jacques, C.A. Cramers, P.J. Schoenmakers, J. High Resolut. Chromatogr. 14 (1991) 438.
[7] A. Rajendran, T.S. Gilkinson, M. Mazzotti, J. Sep. Sci. 31 (2008) 1279.
[8] K. Kaczmarski, J. Kostka, W. Zapała, G. Guiochon, J. Chromatogr. A 1216 (2009) 6560.
[9] J. Kostka, F. Gritti, G. Guiochon, K. Kaczmarski, J. Chromatogr. A 1217 (2010) 4704.
[10] V. Wong, R.A. Shalliker, G. Guiochon, Anal. Chem. 76 (2004) 2601.
[11] T. Farkas, G. Guiochon, Anal. Chem. 69 (1997) 4592.
[12] D. Antos, K. Kaczmarski, W. Piatkowski, A. Seidel-Morgenstern, J. Chromatogr. A 1006 (2003) 61.
[13] G. Guiochon, A. Felinger, A.M. Katti, D. Shirazi, Fundamentals of Preparative and Nonlinear Chromatography, second ed., Elsevier, Amsterdam, 2006.
[14] R.B. Bird, W.E. Stewart, E.N. Lightfoot, Transport Phenomena, John Wiley & Sons, 2002.
[15] D. Horne, J.H. Knox, L. McLaren, Sep. Sci. 1 (1966) 531.
[16] J.H. Knox, G.R. Laird, P.A. Raven, J. Chromatogr. 122 (1976) 129.
[17] D.E. Martire, R.E. Boehm, J. Phys. Chem. 91 (1987) 2433.
[18] R. Span, W. Wagner, J. Phys. Chem. Ref. Data 25 (1996) 1509.
[19] A. Fenghour, W.A. Wakeham, V. Vesovic, J. Phys. Chem. Ref. Data 27 (1998) 1.
[20] V. Vesovic, W.A. Wakeham, G.A. Olchowy, J.V. Sengers, J.T.R. Watson, J. Millat, J. Phys. Chem. Ref. Data 19 (1990) 763.
[21] Y.P. Zarichnyak, V.V. Novikov, Inzhenerno-Fizicheskii Zhurnal 34 (1978) 648.
[22] E.J. Wilson, C.J. Geankoplis, Ind. Eng. Chem. Fundam. 5 (1966) 9.
[23] P.R. Sassiat, P. Mourier, M.H. Caude, R.H. Rosset, Anal. Chem. (Washington, DC, USA) 59 (1987) 1164.
[24] K. Kaczmarski, G. Storti, M. Mazzotti, M. Morbidelli, Comput. Chem. Eng. 21 (1997) 641.
[25] P.N. Brown, A.C. Hindmarsh, G.D. Byrne. Available from: http://www.netlib.org.
[26] J.R. Strubinger, H. Song, J.F. Parcher, Anal. Chem. (Washington, DC, USA) 63 (1991) 98.